

Power curve tracking in the presence of a tip speed constraint

C.L. Bottasso^{*,a}, A. Croce^a, Y. Nam^b, C.E.D. Riboldi^a

^a*Politecnico di Milano, Dipartimento di Ingegneria Aerospaziale
Via La Masa 34, 20156 Milano, Italy*

^b*Kangwon National University, Department of Mechanical Engineering
Chuncheon, Korea*

Abstract

We consider the problem of power regulation for a variable speed wind turbine in the presence of a blade tip speed constraint, for example to limit noise emissions. We formulate a policy in the transition region between the classical regions II and III which accommodates the tip speed constraint, and we derive wind schedules for the rotor speed, blade pitch and aerodynamic torque. Based on these wind schedules, we formulate model-based controllers which are capable of performing power curve tracking throughout all wind speeds, in contrast with commonly adopted approaches which use switching controllers to cover the various operating regimes of the machine. The proposed regulation policies and control laws are demonstrated in a high fidelity simulation environment for a representative 3 MW machine.

Key words: Wind energy, Variable speed wind turbine, Power curve, Noise, Control laws

Notation

\mathbf{u}	Input vector
\mathbf{w}	Wind vector field
\mathbf{x}	State vector
\mathbf{y}	Output vector
$\boldsymbol{\lambda}$	Vector of Lagrange multipliers

*Corresponding author. Tel.: +39-02-2399-8315; Fax: +39-02-2399-8334.

Email address: carlo.bottasso@polimi.it (C.L. Bottasso)

URL: <http://www.aero.polimi.it/bottasso> (C.L. Bottasso)

β	Blade pitch
λ	Tip-speed-ratio
Ω	Rotor speed
ψ	Rotor azimuthal position
ρ	Air density
θ	Yaw angle between nacelle and tower
A	Rotor area
B	Number of blades
C_F	Force coefficient
C_P	Power coefficient
C_T	Torque coefficient
F	Force
J	Cost function
P	Power
R	Rotor radius
T	Torque
V	Mean wind speed, computed by averaging V_w
V_t	Turbulent wind, $V_t = V_w - V$
V_w	Instantaneous wind, $V_w = V + V_t$
t	Time
$(\cdot)^*$	Goal desired quantity
$(\cdot)^T$	Transpose
$(\cdot)_c$	Commanded quantity, as computed by a controller
$(\cdot)_e$	Effective quantity, output by an actuator
$(\cdot)_r$	Rated quantity, i.e. corresponding to the achievement of rated power
$\dot{(\cdot)}$	Derivative with respect to time t , $d(\cdot)/dt$
(\cdot)	Quantity referred to the fine scale model
$(\cdot)^{II}$	Quantity pertaining to region II
$(\cdot)^{II^{1/2}}$	Quantity pertaining to region II ^{1/2}
$(\cdot)^{III}$	Quantity pertaining to region III
$\mathbf{a}_{,b}$	Derivative of vector \mathbf{a} with respect to vector \mathbf{b} , $\partial\mathbf{a}/\partial\mathbf{b}$

1. Introduction

Variable speed wind turbines are regulated according to different policies, depending on the intensity of the mean wind speed. Typically, one may distinguish two main power production regimes (see e.g. [6]).

In the first, called region II, the machine operates at maximum power coefficient, which means that the wind turbine is governed so as to maintain a constant tip speed ratio (TSR) for varying wind speeds; as the wind increases, the rotor angular speed also increases. This regulation policy is obtained by keeping the blade pitch setting fixed at the value of maximum power coefficient, and by modulating the electrical torque so as to trim the machine at the desired rotor speed. In region II, the generated power increases according to a cubic law with increasing wind speed.

A second power production regime is called region III, which begins for a wind intensity, called rated wind, such that the machine reaches rated power. For winds higher than rated, the machine is kept operating at constant rotor speed and constant torque, and hence at constant power. This regulation policy is obtained by pitching the blades so as to adjust the aerodynamic torque at each mean wind speed value.

Power curve tracking in the two regions imply different regulation policies: constant pitch – variable torque for region II, and variable pitch – constant torque in region III. Because of this reason, it is a rather common practice to use switching control laws: two different regulators operate in the two different regions, and switching between the two is performed according to the current wind speed. This means that one has to develop two different controllers; furthermore, there is often the need to devise some kind of blending scheme to avoid too sudden a switching between the two operating regimes, which may cause load peaks or vibrations.

Things become even more complicated for large wind turbines with noise constraints. In fact, since wind turbine generated noise is very well correlated with blade tip speed [16, 13, 3], one of the most effective ways to design relatively quiet wind turbines is to simply place a limit on the blade tip speed (although, clearly, further benefits can be achieved by other means, such as the choice of appropriate airfoils, planform and tip shapes, etc.). For a given rotor radius, a limit on the blade tip speed implies a limit on the rotor speed; for large wind turbines, such a limit is often smaller than the rotor speed necessary to achieve rated power at the end of region II. Consequently, the introduction of an upper limit on rotor speed alters the situation described above of regulation with sole two policies, as one now necessitates of a third *transition* region in between regions II and III [6].

Therefore, in the presence of a blade tip constraint, it is necessary: a) to define a regulation policy in the transition region, and b) to design control laws capable of effective power curve tracking in all these operating regimes. Clearly, the use of switching regulators in this case becomes a little more problematic. In fact, one has now to design three different control laws, and

to devise suitable blending schemes at all transition points from one region to the next.

These problems have received considerable attention in the literature. Particularly relevant to the present discussion are developments in the area of control scheduling, which is used for ensuring appropriate performance across the entire operating range of the machine, by accounting for its regime-dependent dynamics. Among the many possible sources, we mention here Ref. [15] that presents a comprehensive review of gain scheduling techniques, and Ref. [14] which addresses the specific case of scheduling for wind turbine control; furthermore, Ref. [22] describes recent developments within the closely related framework of Linear Parameter Varying (LPV) systems. Often, scheduling of wind turbine controllers is driven by the wind speed, since this enables the same scheduling logic to be used over the entire operating envelope of the machine. Estimates of the wind for this purpose can be obtained by the use of ad hoc estimators, as described for example in Refs. [18, 17, 21, 10].

Within the area of power regulation across the whole wind speed range, described above, the present work has two main goals.

First, we describe a formulation of the transition region, here named region $II^{1/2}$, which accounts explicitly for power production, the presence of the tip speed constraint, and torque-rotor speed stability. The resulting regulation policies in regions II, $II^{1/2}$ and III define smoothly varying wind-dependent regulation set points for the rotor speed, collective blade pitch and rotor torque, throughout the whole range of operating wind speeds. Although regulation policies similar to the one here described are probably used by manufacturers of large (especially on-shore) wind turbines, we are not aware of publications describing in detail how to formulate the transition region.

A second goal of the present work is to develop an example of the use of the proposed regulation policy for the implementation of a scheduled control law. To this end, we consider the case of model-based optimal controllers, which have received considerable attention since almost twenty years for the regulation of wind turbines, as described in Ref. [6] and more recently in Ref. [11]. More specifically, considering the well known case of linear quadratic regulators (LQR) [20, 6], it is shown here how the proposed wind-scheduled policy can be used to define a wind-varying reference for feed-forward control [26, 27] driven by wind estimates [18, 17, 21, 10]. Since, by using this approach, goal regulation quantities vary with continuity across the wind speed range, there is no need to use different controllers in the different operating regimes, nor there is any need to introduce switching

logics or blending schemes to deal with the transitions from one region to the next. In fact, controllers designed on the basis of the proposed wind-scheduled regulation policies are not even aware of the presence of different operating regions: all they deal with are wind scheduled goal regulation states, which vary in a smooth way as the wind speed changes. This comes with a substantial simplification in the formulation, coding, testing and tuning of the control laws.

The paper is organized according to the following plan. At first, we describe wind scheduled regulation strategies, describing policies in region II, II^{1/2} and III. This part is completed by showing rotor speed, pitch and torque wind schedules for a hypothetical representative 3 MW wind turbine, and by illustrating the effect of the transition region on the torque-rotor speed stability of the machine. Next, we formulate both a collective LQR and an individual blade pitch LQR; the latter uses the azimuthal position of the rotor to introduce individual pitch variations for the rotor blades which help in reducing harmonic load components, with a resulting reduced fatigue damage to the structure. It is not the goal of this paper to thoroughly compare these two different LQR formulations between themselves and with other possible approaches; their goal here is just to show that the proposed approach is readily applicable to various model-based controllers, irrespectively of the details of their formulations. Finally, the two controllers are used for demonstrating power curve tracking in a high fidelity simulation environment using a detailed aero-servo-elastic wind turbine model.

2. Wind scheduled regulation strategies

The different wind speed operating regimes of a variable speed wind turbine are named regions I, II and III. In region I, the machine is not yet in a power production mode since the wind is not sufficiently high to maintain the machine in operation.

2.1. Region II regulation

Power production begins at the cut in wind speed, which signals the beginning of region II. The power P can be expressed in general as

$$P = \frac{1}{2} \rho A V^3 C_P(\lambda, \beta), \quad (1)$$

where ρ is the air density, A the rotor area, V the wind speed, C_P the power coefficient, which depends on the TSR $\lambda = \Omega R/V$, with Ω the rotor angular speed and R the rotor radius, while β is the collective blade pitch setting.

In region II, power is maximized by operating for all wind speeds at the maximum value of the power coefficient, which is computed by solving the following optimization problem

$$C_P^{II} = \max_{\lambda, \beta} C_P(\lambda, \beta). \quad (2)$$

The constant (with respect to the wind speed) values of TSR and blade pitch which correspond to the maximum value of the power coefficient C_P^{II} are indicated as λ^{II} and β^{II} , respectively:

$$\lambda^{II}, \beta^{II} = \arg \max_{\lambda, \beta} C_P(\lambda, \beta). \quad (3)$$

Figure 1 shows the behavior of the $C_P - \lambda - \beta$ curves for a hypothetical 3 MW machine, and the values of the optimal parameters C_P^{II} , λ^{II} and β^{II} . The tracing of the curves of Fig. 1 using a comprehensive aero-servo-elastic model is explained later on in §3.3.

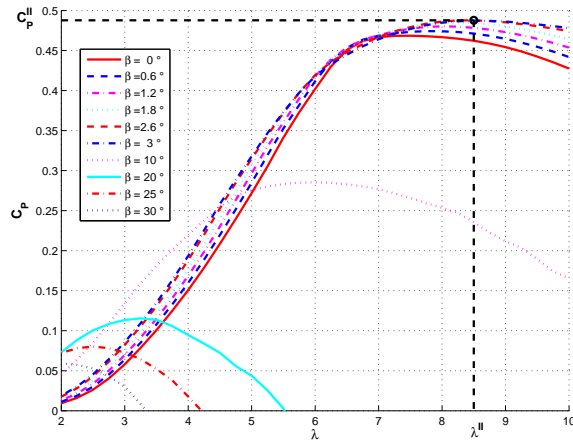


Figure 1: Power coefficient C_P vs. TSR λ for varying collective blade pitch settings β , for a hypothetical 3 MW wind turbine.

Since in region II the TSR is held constant, $\lambda^{II} = \text{const.}$, the rotor angular speed increases linearly with the wind speed V :

$$\Omega(V) = \frac{\lambda^{II} V}{R}. \quad (4)$$

It is readily verified that the power and rotor aerodynamic torque increase

with increasing wind speed as

$$P(V) = \frac{1}{2} \rho A V^3 C_P^{II}, \quad (5a)$$

$$T(V) = \frac{1}{2} \rho A R V^2 \frac{C_P^{II}}{\lambda^{II}}. \quad (5b)$$

2.2. Tip speed constraint and region II/2 regulation

In the absence of blade tip speed constraints, the machine keeps operating in region II until the rated power P_r is reached. The value of the wind speed where the wind turbine reaches rated power is termed rated speed, which is readily computed as

$$V_r = \sqrt[3]{\frac{2P_r}{\rho A C_P^{II}}}. \quad (6)$$

Similarly, the rated rotor speed is the value of Ω assumed by the rotor at the rated wind speed, i.e.

$$\Omega_r = \frac{\lambda^{II}}{R^{5/3}} \sqrt[3]{\frac{2P_r}{\rho \pi C_P^{II}}}. \quad (7)$$

For noise considerations, it is a good design practice to place a limit on the blade tip speed $v_{\text{tip}} = \Omega R$, i.e.

$$v_{\text{tip}} \leq v_{\text{tip}_{\text{max}}}, \quad (8)$$

typical values for on-shore operations being in the range $v_{\text{tip}_{\text{max}}} \approx 72 \div 76$ m/sec [16]. For a given radius R , this constraint translates into a limit to the rotor speed:

$$\Omega \leq \frac{v_{\text{tip}_{\text{max}}}}{R} = \Omega_{\text{max}}. \quad (9)$$

For machines with large rotors, Ω_{max} is typically smaller than Ω_r ; this means that the rated rotor speed can not be reached by regulating the machine using region II policy, if the blade tip speed constraint has to be enforced. In fact, the largest rotor size which does not incur into this problem is

$$R = \left(\frac{\lambda^{II}}{v_{\text{tip}_{\text{max}}}} \sqrt[3]{\frac{2P_r}{\rho \pi C_P^{II}}} \right)^{3/2}, \quad (10)$$

which is typically smaller than the optimal design rotor radius.

To avoid violating the blade tip speed constraint, the machine has to be regulated by maintaining a constant rotor speed once Ω_{\max} has been reached. The wind speed where the maximum rotor speed is achieved indicates the end of region II regulation and the beginning of a new region termed in this work region $II^{1/2}$; the name indicates that it represents a transition region between the classical regions II and III. The wind speed for entrance in the transition region is indicated as $V_{II^{1/2}}$, and it can be computed as $V_{II^{1/2}} = v_{\text{tip}_{\max}}/\lambda^{II}$. The end of region $II^{1/2}$ is achieved when, for sufficiently high winds, the machine achieves rated power, which signals the entrance into region III.

One possible way of regulating the machine in region $II^{1/2}$ is to maximize again the power coefficient, similarly to what done for the region II policy. However, in this case the TSR can not be maintained constant; in fact, since the machine has to be kept operating at a fixed rotor speed, the TSR must decrease for increasing wind speed, i.e.

$$\lambda(V) = \frac{\Omega_{\max}R}{V} = \frac{v_{\text{tip}_{\max}}}{V}. \quad (11)$$

The maximum power coefficient policy is computed by solving the following optimization problem for each wind speed V :

$$\forall V \in [V_{II^{1/2}}, V_r] \quad C_P^{II^{1/2}}(V) = \max_{\beta} C_P(\lambda(V), \beta), \quad (12)$$

which also gives the corresponding collective blade pitch setting:

$$\forall V \in [V_{II^{1/2}}, V_r] \quad \beta^{II^{1/2}}(V) = \arg \max_{\beta} C_P(\lambda(V), \beta). \quad (13)$$

Notice that, differently from the region II case, the blade pitch varies for varying wind. Figure 2 shows the regulation trajectory for C_P in the various operating regions using a thick solid line; the region $II^{1/2}$ segment of the trajectory corresponds to the envelope of the maxima of the $C_P - \lambda - \beta$ curves.

The generated power and torque expressed as functions of the wind speed V are readily computed as

$$P(V) = \frac{1}{2} \rho A v_{\text{tip}_{\max}}^3 \frac{C_P^{II^{1/2}}(V)}{\lambda(V)^3}, \quad (14a)$$

$$T(V) = \frac{P(V)}{\Omega_{\max}}. \quad (14b)$$

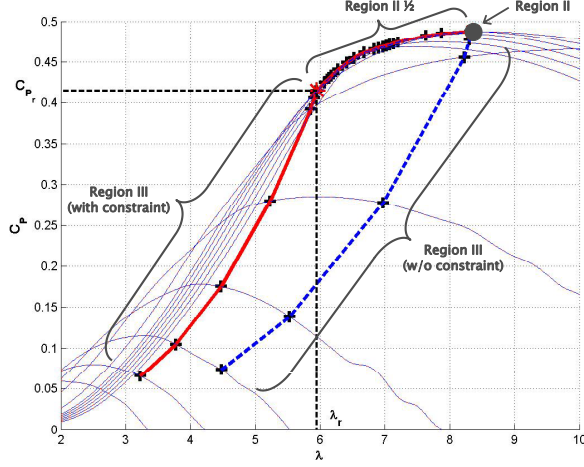


Figure 2: Power coefficient C_P vs. TSR λ for varying collective blade pitch settings β . Thick solid line: regulation trajectory for a machine with tip speed constraint; dashed line: regulation trajectory for a machine without tip speed constraint.

Region III^{1/2} regulation is completed when the machine reaches rated power. The power coefficient for rated power at any TSR is computed from Eq. (14a) as

$$C_P = \frac{2P_r}{\rho A v_{\text{tip,max}}^3} \lambda^3, \quad (15)$$

which is a cubic curve in the $C_P - \lambda$ plane. By intersecting this curve with the envelope of the C_P maxima given by the solution of problem (12), one gets the rated power coefficient $C_{P,r}$, rated TSR λ_r and rated wind speed V_r , which indicate the end of region III^{1/2} regulation (cfr. Fig. 2).

2.3. Region III regulation

The reaching of rated power indicates the end of region III^{1/2} and the beginning of region III. Here the machine is regulated so as to maintain a constant power production as a function of wind speed until the reaching of the cut out wind speed, where the machine is either shut down or progressively slowed down.

Since both power and rotor speed are constant in region III, the aerodynamic torque is also held constant at its rated value

$$T(V) = T_r = \text{const.} \quad (16)$$

In order to achieve this behavior, it is immediately verified that the power coefficient must be varied as a function of the TSR as follows

$$C_P = C_{P_r} \left(\frac{\lambda}{\lambda_r} \right)^3. \quad (17)$$

In turn, the TSR varies as a function of the wind speed as in Eq. (11). The region III segment of the regulation trajectory in the $C_P - \lambda - \beta$ space is shown in Fig. 2.

From the intersection of the region III schedule given by Eq. (17) with the power coefficient curves, one can compute the corresponding values of the collective pitch settings for each TSR, and hence for each wind speed, therefore obtaining the blade pitch wind schedule $\beta = \beta(V)$.

2.4. Rotor speed, pitch and torque wind schedules

From the above discussion, one may readily trace the schedules throughout all operating wind speeds of the optimal regulation set points for the rotor speed, collective blade pitch and rotor aerodynamic torque. Such quantities are of crucial importance, since they will be used as goal regulation values for some of the states (or outputs) and inputs of the machine for the control laws described in Section 3.

Figure 3 shows the schedules for the representative 3 MW machine used in the present study. The figures also report using dashed lines the schedules for a machine without tip speed constraint, which consequently is regulated according to the classical region II and III policies. In this case, one may recognize the constant pitch – variable torque regulation of region II, and the constant torque – variable pitch regulation of region III. On the other hand, in the presence of a blade tip speed constraint, there is a transition region where the machine is regulated according to a variable pitch and torque schedule. Figure 4 shows a zoomed view in region II^{1/2} of the collective blade pitch schedule using a solid line; the pitch schedule in this same wind range is shown using a dashed line for the unconstrained case.

Figure 5 shows the power vs. wind speed curves obtained with (solid line) and without (dashed line) tip speed constraint. Notice the presence of the transition region II^{1/2} for the constrained case. Since the power coefficient in that region is smaller than the one in region II, the power curve is lower in the case of the blade tip constraint. However, at the price of a power decrease, the machine operates in a quieter way; the trade-off between power and noise is a typical design choice, which can be finalized based on the overall design philosophy and on further considerations involving, for example, the

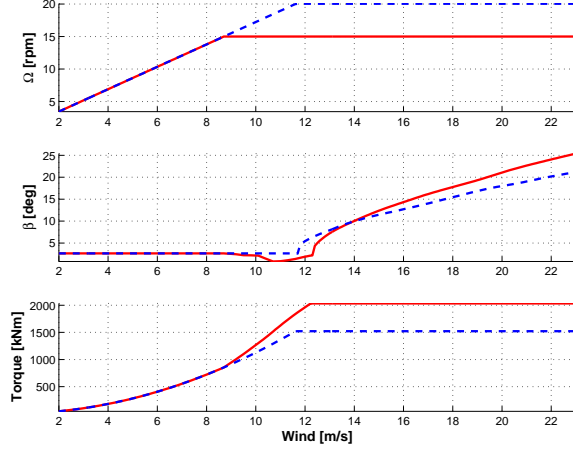


Figure 3: Wind schedules for regulation set points in regions II, II^{1/2} and III. Top: schedule of the rotor speed; center: schedule of the collective blade pitch setting; bottom: schedule of the rotor torque. Dashed lines: schedules for wind turbine without tip speed constraint (pure region II-III regulation).

weighting of the power curve with a target Weibull distribution to assess the impact of the power cut on the annual energy production.

2.5. Rotor speed stability considerations

It should be realized that the introduction of a blade tip speed constraint may impact the torque-speed stability of the machine. To illustrate this fact, Fig. 6 shows the curves of the torque coefficient C_T as a function of the TSR λ for varying collective blade pitch settings β , where

$$T = \frac{1}{2} \rho A R V^2 C_T, \quad (18)$$

and $C_T = C_P/\lambda$.

In region II, the machine is regulated at a constant torque coefficient. In fact, since both $\lambda = \lambda^{II} = \text{const.}$ and $C_P = C_P^{II} = \text{const.}$, then also $C_T = C_P/\lambda = C_T^{II} = \text{const.}$ (although the torque is not constant). On the other hand, using Eq. (17), the torque coefficient in region III changes as

$$C_T = C_{T_r} \left(\frac{\lambda}{\lambda_r} \right)^2. \quad (19)$$

Figure 6 shows the regulation trajectory in the $C_T - \lambda$ plane for the pure region II–III policy using a thick dashed line. It appears that the machine

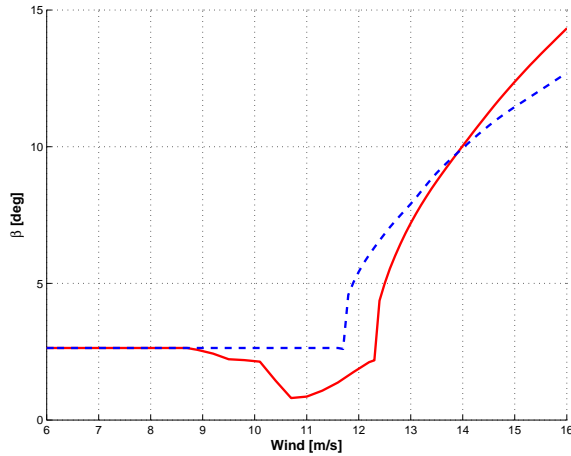


Figure 4: Zoomed view of collective blade pitch schedule for regulation set points around region $\text{II}^{1/2}$. Thick solid line: schedule for a machine with tip speed constraint; dashed line: schedule for a machine without tip speed constraint.

operates at all times in regions of the plane where the $C_T - \lambda$ curves have a negative slope, which is indicative of a (statically) stable behavior with respect to perturbations in the rotor speed.

For a machine with tip speed constraint, regulation in region $\text{II}^{1/2}$ implies a movement towards the left in the $C_T - \lambda$ plane, until rated torque is reached (passed that point, the regulation reverts back to the region III strategy, and the torque coefficient obeys once again to Eq. (19)). This movement may imply a significant loss of stability, and the possible encounter of regions of unstable behavior (positive $C_T - \lambda$ curve slopes). This fact is illustrated once again by Fig. 6, which shows the regulation trajectory in the constrained case using a thick solid line. It appears that the machine operates in an unstable regime right before entering in region III.

Two considerations are in order with respect to this point. First, the loss of stability can be mitigated by reducing the uphill motion on the $C_T - \lambda$ curves in region $\text{II}^{1/2}$; this may be achieved by choosing lower values of the power coefficients in that region, i.e. by abandoning the optimal C_P policy given by Eq. (12). Clearly, this will come at the cost of a reduced generated power. Second, since the machine is going to be operated in closed-loop, the loss of stability might not be an issue if a suitable feedback control law is employed to stabilize the machine in those operating regimes. For example, for the case of the machine object of the present study using the control laws described below, we have observed a perfectly acceptable closed-loop

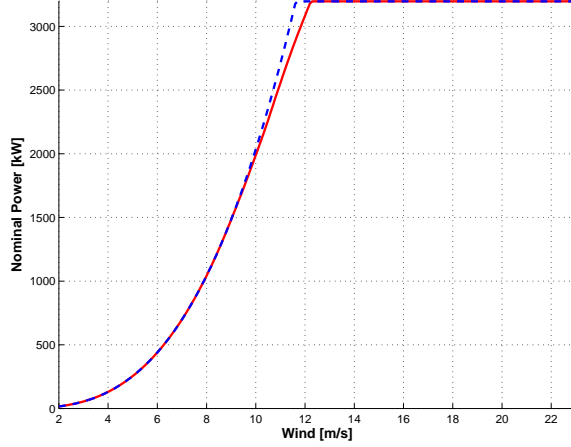


Figure 5: Power vs. wind speed curve. Solid line: machine with tip speed constraint using region II, II^{1/2} and III regulation; dashed line: machine without tip speed constraint using pure region II and III regulation.

behavior of the machine even when operating in turbulent winds in the unstable $C_T - \lambda$ region.

3. Power curve tracking using linear quadratic regulators

3.1. Collective pitch LQR

We consider a wind-scheduled multi-input-multi-output (MIMO) LQR, based on a collective-pitch non-linear wind turbine reduced model which includes drive-train shaft dynamics, elastic tower fore-aft motion, blade pitch actuator dynamics and electrical generator dynamics:

$$(I_{LSS} + I_{HSS})\dot{\Omega} + T_l(\Omega) + T_{el_e} - T_a(\Omega, \beta_e, V_w - \dot{d}, V) = 0, \quad (20a)$$

$$M_T\ddot{d} + C_T\dot{d} + K_Td - F_a(\Omega, \beta_e, V_w - \dot{d}, V) = 0, \quad (20b)$$

$$\ddot{\beta}_e + 2\xi\omega\dot{\beta}_e + \omega^2(\beta_e - \beta_c) = 0, \quad (20c)$$

$$\dot{T}_{el_e} + \frac{1}{\tau}(T_{el_e} - T_{el_c}) = 0. \quad (20d)$$

The first equation, Eq. (20a), describes the drive-train dynamics, where d is the tower top fore-aft displacement and β_e is the effective blade pitch angle. The tower motion d can be reconstructed on-line by using observers from measurements provided by an accelerometer and a strain gage, as described in Ref. [10]. Moreover, I_{LSS} is the sum of the moments of inertia about

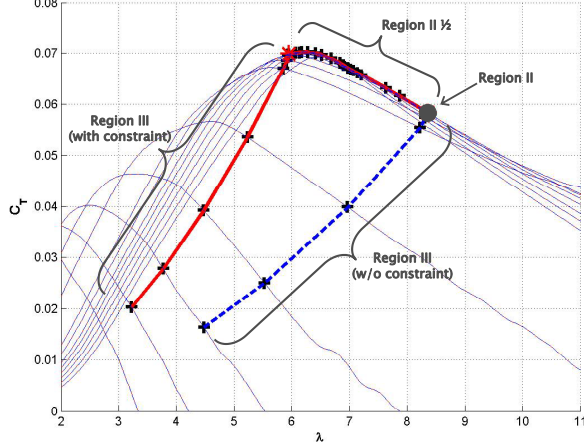


Figure 6: Torque coefficient C_T vs. TSR λ for varying collective blade pitch settings β . Thick solid line: regulation trajectory for a machine with tip speed constraint; dashed line: regulation trajectory for a machine without tip speed constraint.

the rotation axis of the rotor hub and of the three rotor blades (low speed shaft inertia), while I_{HSS} is the moment of inertia of the rotating part of the electric generator and of the high speed shaft referred to the low speed shaft. The torques acting upon the drive-train include the mechanical losses on the shaft bearings T_l , the effective electrical reaction torque T_{el_e} referred to the low speed shaft and the aerodynamic torque T_a . The mechanical loss T_l is modeled by means of a speed-torque look-up table. The second equation, Eq. (20b), models the fore-aft tower dynamics. Here, M_T , C_T and K_T are, respectively, the tower equivalent modal mass, structural damping and bending stiffness, which may be computed by modal reduction of a detailed finite element model of the tower. Finally, F_a indicates the aerodynamic force generated by the rotor. The third equation, Eq. (20c), is a second order model of the blade pitch actuator, where ω is the undamped natural frequency, ξ the damping factor, and β_c the blade pitch control input. The model also includes upper and lower limits on the pitch and the pitch rate. The fourth and last equation, Eq. (20d), is a first order model of the electrical generator that includes a time delay τ , while T_{el_c} is the commanded electrical torque input.

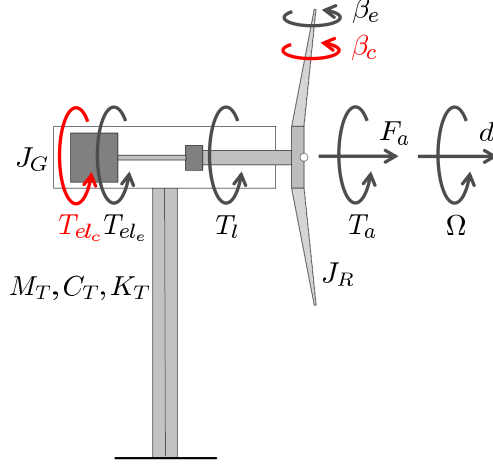


Figure 7: Topological representation of 6 state - 2 input collective-pitch-only model.

The rotor aerodynamic force and torque are computed as

$$T_a = \frac{1}{2} \rho A R \frac{C_P(\hat{\lambda}, \beta_e, V)}{\hat{\lambda}} (V_w - \dot{d})^2, \quad (21a)$$

$$F_a = \frac{1}{2} \rho A C_F(\hat{\lambda}, \beta_e, V) (V_w - \dot{d})^2, \quad (21b)$$

where C_P and C_F are the power and force coefficients, respectively, and $\hat{\lambda}$ is the corrected TSR, defined as $\hat{\lambda} = \Omega R / (V_w - \dot{d})$, i.e. the TSR which accounts for the apparent wind due to the tower fore-aft motion. Finally, $V_w = V + V_t$ is the turbulent upstream wind speed obtained as the sum of the mean wind V and the turbulent wind V_t . For this reduced model, the mean wind V is computed by spatially averaging over the rotor disk the wind speed profile given by the power law [1, 2]. Similarly, the longitudinal turbulent wind V_t is defined, at each time step, as the spatial average over the rotor disk of the Kaimal turbulence model centered at the hub. The dependence of the power and force coefficients in Eqs. (21a) and (21b) on the wind speed V , typically neglected, accounts for the possible effects due to the deformability of tower and blades under high winds.

Equations (20) can be written in compact form as

$$\mathbf{f}(\dot{\mathbf{x}}, \mathbf{x}, \mathbf{u}, \mathbf{w}, t) = 0, \quad (22a)$$

$$\mathbf{y} = \mathbf{h}(\mathbf{x}), \quad (22b)$$

by defining state and input vectors

$$\mathbf{x} = (d, \dot{d}, \Omega, \beta_e, \dot{\beta}_e, T_{el_e})^T, \quad (23a)$$

$$\mathbf{u} = (\beta_c, T_{el_c})^T, \quad (23b)$$

where $\mathbf{w} = (V, V_w)$ is a vector of wind parameters and \mathbf{y} are outputs to be defined later on.

Although the model is rather simple, its accuracy can be substantially enhanced by a proper modeling of the crucial aerodynamic coefficients C_P and C_F . In this work, these coefficients are computed off-line using the fine-scale aero-servo-elastic model, and then stored in tabulated form, the entries of the table being $\hat{\lambda}$ and the blade pitch β_e (and possibly the mean wind speed V if one wants to account for flexibility effects on the rotor power and force coefficients). This way, the reduced model inherits the aerodynamic modeling of the fine scale solver, while keeping a very simple implementation and extremely low computational cost. The estimation of the aerodynamic coefficients is explained in §3.3, employing the same procedure used for the determination of the regulation set points described in Section 2.

The controller operates with the same logic in region II, II^{1/2} and III, by tracking goal regulation states $\mathbf{x}^*(V)$ (or outputs $\mathbf{y}^*(V)$) and control inputs $\mathbf{u}^*(V)$, given in terms of the mean wind V and computed as explained in Section 2. Specifically, for the 3 MW machine used in the present work, Fig. 3 gives the goal regulation rotor speed $\Omega^*(V)$ (top), goal regulation collective pitch setting $\beta_e^*(V) = \beta_c^*(V)$ (center), and goal regulation rotor torque $T_{el_e}^*(V) = T_{el_c}^*(V)$ (bottom) as a function of wind speed. The definition of $\mathbf{x}^*(V)$ is completed by choosing $d^*(V)$ as the computed tower tip deflection at each wind speed, and then simply setting $\dot{d}^*(V) = \dot{\beta}_e^*(V) = 0$.

Notice that there is no switching logic in the controller when transitioning from one region to another: the control law simply tries to regulate the machine around set points for states (or outputs) and inputs, which have been computed as functions of the mean wind speed V . Since these set points vary smoothly throughout the whole operating regime of the machine, there is no need to introduce switching logics at the level of the feedback controller, therefore greatly easing its implementation and tuning.

In order to pick at each instant of time the necessary value of the regulation set point, one needs a measurement of the wind speed. Measurements of the instantaneous turbulent hub-height wind V_w is either provided by the on-board anemometer or, better, by a hub wind observer [18, 17, 21, 9, 10]. The use of a wind estimate to adjust the regulation set points amounts to the introduction of a feed-forward term in the control loop, as described in

Refs. [26, 27]. In this work, the feed-forward mean hub-height wind V is computed with a moving average of the estimated instantaneous wind V_w on a window of 10 seconds.

The goal states and inputs (set points) are computed off-line using the strategies of Section 2 at a certain number of trim points denoted by the wind speeds V_k , $k = 1, \dots, N_{\text{trim}}$, with the fine-scale aero-servo-elastic model. At each one of the trim points, a linearized reduced model is computed from the non-linear one expressed by Eqs. (22). This defines a wind-parameterized reduced linear model

$$\Delta \dot{\mathbf{x}} = \mathbf{A}(V_{w_k})\Delta \mathbf{x} + \mathbf{B}(V_{w_k})\Delta \mathbf{u}, \quad (24a)$$

$$\Delta \mathbf{y} = \mathbf{C}(V_{w_k})\Delta \mathbf{x}, \quad (24b)$$

with $\Delta \mathbf{x} = \mathbf{x} - \mathbf{x}^*(V_k)$, $\Delta \mathbf{u} = \mathbf{u} - \mathbf{u}^*(V_k)$, $\Delta \mathbf{y} = \mathbf{y} - \mathbf{y}^*(V_k)$, and where $\mathbf{A} = \partial \mathbf{f} / \partial \mathbf{x}$, $\mathbf{B} = \partial \mathbf{f} / \partial \mathbf{u}$ and $\mathbf{C} = \partial \mathbf{h} / \partial \mathbf{x}$ are matrices of partial derivatives evaluated at the trim points. Clearly, \mathbf{A} , \mathbf{B} and \mathbf{C} depend on \mathbf{x}^* and \mathbf{u}^* , but this is not reflected in the notation not to excessively clutter it.

Notice that the trim point states, outputs and inputs $\mathbf{x}^*(V_k)$, $\mathbf{y}^*(V_k)$ and $\mathbf{u}^*(V_k)$ are parameterized in terms of the mean wind V_k . In this sense, fluctuations in the instantaneous wind V_w caused by wind turbulence do not imply the change to a new regulation state; in fact, change to a new regulation state should only be caused by changes in the mean wind. On the other hand, the matrices of partial derivatives in Eqs. (24) depend on the instantaneous wind V_{w_k} (cfr. Eqs. (20a) and (20b)).

A quadratic cost function for the regulation problem at the trim point is defined as

$$J = \frac{1}{2} \int_0^\infty (\Delta \mathbf{y}^T \mathbf{Q} \Delta \mathbf{y} + \Delta \mathbf{u}^T \mathbf{R} \Delta \mathbf{u}) dt, \quad (25)$$

where $\mathbf{Q} \geq 0$ and $\mathbf{R} > 0$ are symmetric matrices of weights which may be scheduled in terms of the mean wind V , i.e. $\mathbf{Q} = \mathbf{Q}(V)$, $\mathbf{R} = \mathbf{R}(V)$; tuning of the weights for specific goal-oriented performance is explained in Ref. [9]. The scheduling of the weight matrices with respect to the wind speed accounts for the changes in the operating conditions of the machine for increasing wind, and can help in improving performance. We remark again however, that in the present implementation the same control structure and logic is used throughout the whole operating range of wind speeds, with no specific account for the fact that the machine crosses different operating regimes denoted by different regulation policies.

For full state feedback control ($\mathbf{y} \equiv \mathbf{x}$ in Eq. (24b)) the LQR feedback gain matrix $\mathbf{K}(V_{w_k})$ is computed by solving the steady state (algebraic)

Riccati equation [20]. For output feedback control, the feedback gain matrix is computed based on the procedure of Ref. [19]; output feedback is used when the tower tip deflection and velocity estimates are not available, for example because of a failure in the necessary sensors. The gain matrices at all trim points $\mathbf{K}(V_{w_k})$ are stored in table look-up form, together with the regulation quantities $\mathbf{x}^*(V_k)$ (or $\mathbf{y}^*(V_k)$) and $\mathbf{u}^*(V_k)$.

The closed-loop controller is implemented on-line as

$$\mathbf{u} = -\mathbf{K}(V_w)(\mathbf{y} - \mathbf{y}^*(V)), \quad (26)$$

where the gain matrix at the current instantaneous wind V_w is obtained by linear interpolation of the stored gain matrices at the trim points k and $k + 1$, i.e.

$$\mathbf{K}(V_w) = (1 - \xi)\mathbf{K}(V_{w_k}) + \xi\mathbf{K}(V_{w_{k+1}}), \quad (27)$$

with $\xi = (V_w - V_{w_k})/(V_{w_{k+1}} - V_{w_k})$, $V_w \in [V_{w_k}, V_{w_{k+1}}]$, while the regulation state at the current mean wind V is obtained by linear interpolation of the stored regulation states at the trim points l and $l + 1$, i.e.

$$\mathbf{y}^*(V) = (1 - \eta)\mathbf{y}^*(V_l) + \eta\mathbf{y}^*(V_{l+1}), \quad (28)$$

where $\eta = (V - V_l)/(V_{l+1} - V_l)$, $V \in [V_l, V_{l+1}]$. When using full state feedback in Eq. (26), the tower states in the state vector \mathbf{x} are reconstructed using the Kalman observer described in Ref. [10].

3.2. Individual blade pitch LQR

Individual blade pitch can be used to account for the non-uniform spatial distribution of wind on the rotor disk and for the flow not being aligned with the rotor axis; hence, individual blade pitch control can help in reducing the oscillatory components of the loads, which in turn has a beneficial effect on the fatigue life of the machine.

An individual blade pitch MIMO LQR controller may be formulated using the reduced model depicted in Fig. 8, which gives a sketch of its topological configuration. The model state vector is defined as

$$\mathbf{x} = (\theta, \dot{\theta}, \psi, \dot{\psi}, \dots, \beta_{e_i}, \dot{\beta}_{e_i}, \dots, \mathbf{q}_t^T, \dot{\mathbf{q}}_t^T, \dots, \mathbf{q}_{b_i}^T, \dot{\mathbf{q}}_{b_i}^T, \dots, T_{el_e})^T, \quad i = 1, \dots, B, \quad (29)$$

where θ is the nacelle yaw angle with respect to the tower, ψ the rotor azimuthal angle and $\dot{\psi} = \Omega$, β_{e_i} the blade pitch setting of the i th of the B rotor blades, $i = 1, \dots, B$. The elastic deformations of the tower are

described in terms of tower modal amplitudes \mathbf{q}_t , as done for example in the FAST code [12]; alternatively, \mathbf{q}_t may represent rotations in equivalent hinges used for modeling the first bending mode of the tower in the fore-aft and side-side directions and the first torsional mode, as done in the SymDyn code [25]. Similarly, \mathbf{q}_{b_i} are modal amplitudes of the i th blade, or rotations in equivalent flap hinges. The tower and blade flexible states can be reconstructed on-line with observers by filtering measurements from accelerometers and strain gages [10]. The model input vector is

$$\mathbf{u} = (\theta_c, \dots, \beta_{c_i}, \dots, T_{el_c})^T, \quad i = 1, \dots, B, \quad (30)$$

where θ_c is the commanded yaw angle, β_{c_i} the commanded pitch setting of the i th blade, and T_{el_c} the commanded generator torque.

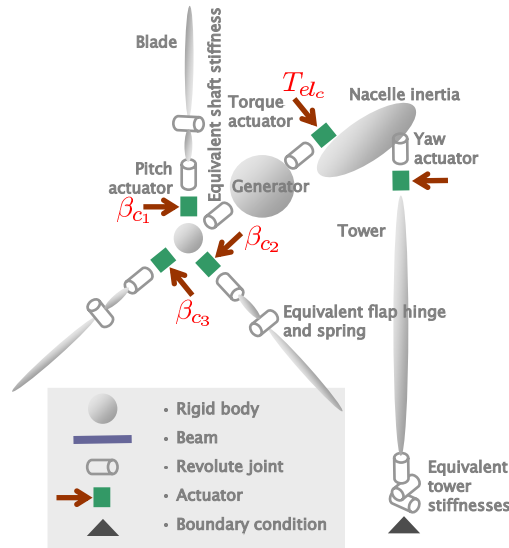


Figure 8: Topological representation of 9 state - 4 input individual blade pitch model.

The equations of motion of the model can be expressed in compact form as

$$\mathbf{f}(\dot{\mathbf{x}}, \mathbf{x}, \mathbf{u}, \mathbf{w}) = \mathbf{f}(\dot{\psi}, \dot{\bar{\mathbf{x}}}, \psi, \bar{\mathbf{x}}, \mathbf{u}, \mathbf{w}) = 0, \quad (31)$$

where in the second expression of the equations we have set $\mathbf{x} = (\psi, \bar{\mathbf{x}}^T)^T$ to put into evidence the presence of the rotor azimuthal position ψ , where $\bar{\mathbf{x}}$ are all states of the model except for the azimuth.

As for the collective LQR regulator, even the present controller operates with the same logic across the whole range of wind speeds, by tracking

goal regulation states $\bar{\mathbf{x}}^*(V)$ (or outputs $\mathbf{y}^*(V)$) and control inputs $\mathbf{u}^*(V)$. Here again, all crucial goal regulation values are given by Fig. 3, while to complete the definition of $\bar{\mathbf{x}}^*(V)$ one simply needs to compute the average (over a rotor revolution) values of the flexible states \mathbf{q}_t and \mathbf{q}_{b_i} at all wind speeds of interest.

At each trim point a linearized reduced model is computed from the non-linear one, written as

$$\Delta \dot{\mathbf{x}} = \mathbf{A}(\psi, V_{w_k}) \Delta \mathbf{x} + \mathbf{B}(\psi, V_{w_k}) \Delta \mathbf{u}, \quad (32a)$$

$$\Delta \mathbf{y} = \mathbf{C}(\psi, V_{w_k}) \Delta \mathbf{x}. \quad (32b)$$

Notice that in this case the matrices of partial derivatives are periodic, since they depend on the azimuthal position of the rotor.

Here again, the trim point states and inputs $\mathbf{x}^*(V_k)$ and $\mathbf{u}^*(V_k)$ are parameterized in terms of the mean wind V_k , while the partial derivatives $\mathbf{A}(\psi, V_{w_k})$, $\mathbf{B}(\psi, V_{w_k})$ and $\mathbf{C}(\psi, V_{w_k})$ depend on the instantaneous wind V_{w_k} .

Based on the cost function of Eq. (25), there are several different ways to compute a feedback law [9]. In this work, the computation of optimal full state feedback gains is based on the azimuthal averaging approach. The matrices of partial derivatives $\mathbf{A}(\psi, V_{w_k})$ and $\mathbf{B}(\psi, V_{w_k})$ are averaged over a rotor revolution to remove the dependence on ψ , i.e.

$$\mathbf{A}_{\text{ave}}(V_{w_k}) = \frac{1}{2\pi} \int_0^{2\pi} \mathbf{A}(\psi, V_{w_k}) d\psi, \quad (33a)$$

$$\mathbf{B}_{\text{ave}}(V_{w_k}) = \frac{1}{2\pi} \int_0^{2\pi} \mathbf{B}(\psi, V_{w_k}) d\psi. \quad (33b)$$

Next, the steady state Riccati equation is solved to get the gain matrix $\mathbf{K}_{\text{ave}}(V_{w_k})$, for which the implementation of the closed-loop law is as in Eq. (26).

The output feedback case is also of interest, since not all state estimates could always be available, for example in case of sensor failures; an output feedback formulation allows the continued operation of the machine, although with a possibly less performing feedback control law. Even in this case, averaging is used for removing the dependence of the matrices on the azimuthal rotor angle, and the optimal feedback gains are computed according to the procedure of Ref. [19].

3.3. Tracing of $C_P - \lambda - \beta$ curves

When a wind turbine operates in constant (in time) wind conditions, the machine settles on a periodic orbit (trimmed operating condition). The

periodicity of the response is caused by the non-uniformity of the spatial distribution of the wind over the rotor disk, which is due to the vertical wind shear (Earth boundary layer), possible lateral shear, and tower shadow effect, and to the fact that the wind direction is in general not parallel to the rotor axis, due to the rotor up-tilt and the possible presence of lateral (operation in yawed conditions) and vertical wind components (e.g., due to the terrain orography in proximity of the wind turbine). The vertical wind shear, tower shadow and rotor up-tilt are always present, while the other effects may or may not exist depending on the operating conditions of the machine.

As previously described, the definition of regulation strategies (Section 2) and control laws (Section 3) necessitates of the knowledge of the zeroth harmonic term (average over a rotor revolution) of the response of certain states and of the inputs, which in turn enable one to compute the $C_P - \lambda - \beta$ and $C_T - \lambda - \beta$ curves of the machine. It is a common practice to compute such fundamental operating curves of a wind turbine using an *isolated rigid rotor*, by considering axial flow conditions and a uniform distribution of the wind over the rotor, since this yields a steady rather than periodic response.

We have found that an improved behavior of the controllers can be obtained by computing such quantities using a complete flexible wind turbine model, rather than the isolated rigid rotor. We use a complete aero-servo-elastic model of the machine implemented in the software program described later on in this document, model which includes flexible blades and tower, rotor up-tilt, vertical wind shear layer and tower shadow effect.

Using this model, which captures the principal causes for a periodic response of the machine, transient simulations could be run for given values of the wind speed, blade pitch setting and generator torque. Once the solution settles on a periodic orbit, the zeroth harmonic of all quantities of interest could be computed, including values of the power coefficient and TSR. Although this would clearly be the most accurate way of computing the $C_P - \lambda - \beta$ curves, in reality this approach creates a chicken and egg problem, because one necessitates of a regulator capable of trimming the machine at each operating point of interest for computing those very curves necessary for formulating the controller. While this problem may be overcome for machines without tip speed constraints (pure region II-III regulation), since one may use simple PID regulators for tracing the curves necessary for the definition of the LQR ones, this proves substantially more difficult for machines with tip speed constraints. In fact, in that case the presence of the transition region II^{1/2} which necessitates of a coupled torque and pitch control, makes it difficult to quickly formulate simple regulators

for the sole problem of curve tracing.

To address this issue, and still allow the computation of the $C_P - \lambda - \beta$ curves with a detailed flexible wind turbine model, we have devised the following procedure. Instead of conducting transient simulations, we perform static solutions for varying wind speeds, rotor speeds and blade pitch settings. During such simulations, we compute the deflected wind turbine configuration under the action of the steady aerodynamic and inertial loads due to a steady rotation of the rotor at a constant angular speed. The simulation also include all other steady loads, such as gravity, wind loads on the tower and nacelle, and blade-tower aerodynamic interference loads. In practice, such simulation amounts to a snap-shot of the wind turbine at a given rotor azimuthal position, where accelerations have been neglected except for the inertial loads caused by a constant rotor speed. Each one of these simulations is extremely fast to compute, since it amounts to a simple (although non-linear) static solution. By computing the solution at different values of the rotor azimuthal angle, one obtains a quasi-static picture of the periodic response of the rotor around a full revolution. Averaging over the rotor revolution, one obtains quasi-static estimates of the necessary quantities (C_P , C_T , etc.). Notice that such estimates are obtained using a complete flexible model of the wind turbine which includes all principal causes for a period response, without necessitating the use of a regulator. Clearly, by repeating such computations for varying values of the TSR and blade pitch, one can obtain the complete $C_P - \lambda - \beta$ curves, as for example those shown in Fig. 1.

3.4. Wind turbine plant model and virtual testing environment

Figure 9 depicts the virtual testing environment used in this work for the tuning and testing of control laws. Aero-servo-elastic models of wind turbines are implemented with the software Cp-Lambda (Code for Performance, Loads and Aeroelasticity by Multi-Body Dynamic Analysis), based on a finite-element-based multibody formulation (see Ref. [4] and references therein). The multibody formulation is based on the full finite-element method, which means that no modal-based reduction is performed on the deformable components of the structure. Cartesian coordinates are used for the description of all entities in the model, and all degrees of freedom are referred to a single inertial frame; the formulation handles arbitrarily large three-dimensional rotations.

The turbine blades and tower are modeled using geometrically exact, composite-ready beams. The element models beams of arbitrary geometry, including curved and twisted reference lines, and accounts for axial, shear,

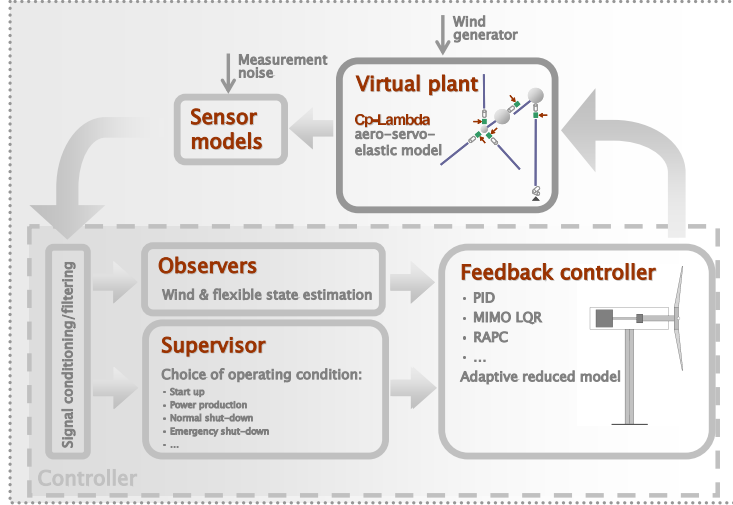


Figure 9: Virtual testing environment.

bending, and torsional stiffness. Joints are modeled through holonomic or nonholonomic constraints, as appropriate, which are enforced by means of Lagrange multipliers using the scaled augmented Lagrangian method [8]. All joints can be equipped with internal springs, dampers, backlash, and friction models.

Lifting lines can be associated with beam elements and are described by three-dimensional twisted curves, which do not necessarily coincide with the associated beam reference lines. The lifting lines are based on classical two-dimensional blade element theory and use local profile aerodynamic characteristics, accounting for the aerodynamic center offset, twist, sweep, and unsteady corrections. Lifting lines are used here to model the aerodynamic characteristics of the blades, but also of the tower and of the nacelle. An inflow element can be associated with the blade lifting lines to model the rotor inflow effects; presently, the code implements the Peters-He dynamic inflow wake model [23] and a classical blade-element momentum (BEM) model based on the annular stream-tube theory with wake swirl. Tip and hub loss models are also considered.

Wind is modeled as the sum of a steady state mean wind and a perturbation wind, accounting for turbulence and/or gusts. The deterministic component of the wind field implements the transients specified by IEC 61400 [1, 2], the exponential and logarithmic wind shear models, and the tower shadow effects, which include the potential flow model for a conical

tower, the downwind empirical model based on Ref. [24], or an interpolation of these two models. The stochastic component of the wind field is computed according to the Mann or Kaimal turbulence models. The turbulent wind is precomputed before the beginning of the simulation for an assigned duration of time and for a user-specified two-dimensional grid of points. During the simulation, the current position of each airstation is mapped to this grid, and the current value of the wind is interpolated in space and time from the saved data.

The multibody formulation used in this effort leads to a set of non-linear partial differential algebraic equations. Spatial discretization of the flexible elements of the model using the finite-element method yields a system of differential algebraic equations in time. Hence, after spatial discretization, a generic wind turbine aero-servo-elastic multibody model \mathcal{M} can be written as

$$\tilde{\mathbf{f}}_{\text{SD}}(\tilde{\mathbf{x}}_{\text{SD}}, \tilde{\mathbf{x}}_{\text{SD}}, \tilde{\boldsymbol{\lambda}}, \tilde{\mathbf{x}}_{\text{C}}, \mathbf{u}, t) = 0, \quad (34\text{a})$$

$$\tilde{\mathbf{c}}(\tilde{\mathbf{x}}_{\text{SD}}, t) = 0, \quad (34\text{b})$$

$$\tilde{\mathbf{f}}_{\text{C}}(\tilde{\mathbf{x}}_{\text{C}}, \tilde{\mathbf{x}}_{\text{C}}, \tilde{\mathbf{x}}_{\text{SD}}, \mathbf{u}, \mathbf{w}, t) = 0, \quad (34\text{c})$$

$$\tilde{\mathbf{y}} = \tilde{\mathbf{h}}(\tilde{\mathbf{x}}_{\text{SD}}, \tilde{\mathbf{x}}_{\text{C}}), \quad (34\text{d})$$

where $\tilde{\mathbf{x}}_{\text{SD}}$ are the structural dynamics states, $\tilde{\boldsymbol{\lambda}}$ are constraint-enforcing Lagrange multipliers, $\tilde{\mathbf{x}}_{\text{C}}$ are the states describing the coupled fields (e.g. aerodynamic, hydraulic, etc.), \mathbf{u} is the control input vector, the wind is given by a vector field $\mathbf{w} = \mathbf{w}(\mathbf{r}, t)$ which depends on space \mathbf{r} and time t . Equations (34a) group together the equations of dynamic equilibrium and the kinematic equations. Equations (34b) represent mechanical joint constraint equations, while Eqs. (34c) are the coupled physics governing equations. Finally, Eqs. (34d) define a set of output quantities $\tilde{\mathbf{y}}$.

Equations (34) are solved using an implicit integration procedure that is nonlinearly unconditionally stable [7, 5]. The implicit nature of the scheme allows for the use of large time steps and is more appropriate than explicit schemes for the typical dynamics of rotor systems. At each time step, the resulting nonlinear system of equations is solved using a quasi-Newton scheme. The time-step length is adjusted based on an error indicator.

The code supports static and transient analyses, and the computation of eigenfrequencies and eigenmodes about deformed equilibrium configurations. Automated procedures support a number of standard operations, such the computation of Campbell diagrams, the automated analysis of all IEC 61400 design load cases (DLCs) [1, 2], the determination of trimmed

periodic conditions, the generation of C_P vs. tip-speed-ratio (TSR) curves, the tracing of power curves, the determination of fatigue equivalent loads using rain-flow analysis, etc.

4. Numerical simulations

The regulation strategies described above were used for computing the power curve in turbulent wind of a 3 MW wind turbine, using the collective and individual blade LQR controllers. The blade tip speed was limited to $v_{\text{tip}_{max}} = 74$ m/sec. Accordingly, the machine regulation schedule was obtained as discussed in Section 2, with the resulting quantities shown by Figs. 1 through 6.

Figure 10 shows the power vs. wind speed curve. The dashed line is the nominal curve already shown in Fig. 5, i.e. the curve obtained from the regulation trajectory and $C_P - \lambda - \beta$ curves of Fig. 2. The figure also shows the power curves obtained with the two LQR controllers operating in class B turbulent winds, the solid line indicating the collective case and the dash-dotted line referring to the individual pitch case. To obtain these curves, simulations of 600 sec were conducted according to the IEC 61400 DLC 1.1 [1, 2] for varying values of the mean wind speed and for class B turbulence using the Kaimal model. The figure shows a good tracking of the power curve in turbulent winds, demonstrating the capability of the controller to regulate the machine at the desired goal set points throughout the whole range of operating regimes.

The decrease in power with respect to the nominal case is primarily due to the enforcement at all times of the upper limit $T \leq 1.1 T_r$ on the electric torque, introduced to avoid overstressing the drive-train system with excessive torque peaks. Limiting the electrical torque creates an asymmetry with respect to power fluctuations above and below the nominal value. In fact, for wind speed fluctuations below the average wind, less power will be generated because the aerodynamic torque and possibly the rotor speed decrease with respect to their nominal values; on the other hand, for wind speed fluctuations above the average wind, the electric torque may hit its maximum allowable limit. Hence, what is lost in terms of generated power during the low wind fluctuations, can not be regained during high speed fluctuations, which explains why the turbulent power curve can not reach the nominal power curve, irrespectively of the efficacy of the feedback control law. Clearly, this effect is more pronounced for increasing intensity of the turbulence, since this will imply larger fluctuations of the wind speed around its mean value.

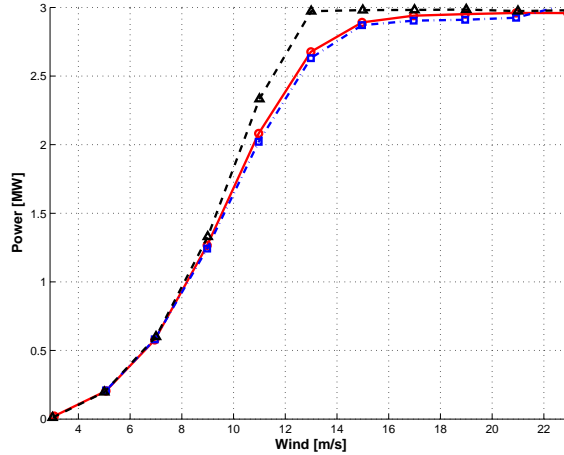


Figure 10: Power vs. wind speed curve. Solid line: collective LQR controller operating in class B turbulent wind; dash-dotted line: individual blade pitch LQR controller operating in class B turbulent wind; dashed line: nominal curve in constant-in-time wind.

5. Concluding remarks

In this paper we have studied the problem of regulating a variable speed wind turbine in the presence of a blade tip speed constraint. Such constraints, which are used for reducing noise emissions, typically limit the rotor speed to a value which is lower than the one necessary for achieving rated power at the end of region II. Therefore, there is the need to define a transition region, capable of bringing the machine to the production of rated power while satisfying the rotor speed constraint. We have formulated such a regulation policy, and we have demonstrated power curve tracking with two representative model-based controllers.

On the basis of the results obtained, the following conclusions maybe drawn:

- The proposed region II^{1/2} transition policy amounts to a coupled pitch-torque control, which generates a smooth transition between region II and region III of the set points for rotor speed, blade pitch and rotor torque.
- Region II^{1/2} policy may be based on the optimization of the power coefficient, which maximizes power production during the transition. This often implies a significant loss in the static torque-rotor speed stability. Although this should not be an issue since the machine

always operates under closed-loop feedback control, increased static stability may be obtained by abandoning the optimal power coefficient policy at the cost of a somewhat reduced produced power.

- Wind schedules of rotor speed, blade pitch and rotor torque can be used as regulation set points for the design of control laws operating without switchings across the whole operating range of wind speeds. The resulting controllers are simple to formulate and implement, and appear to work effectively in all operating regimes. The tuning parameters of such controllers may be optimized in terms of the wind speed for further performance improvements (wind scheduled gains), although in the present case we are able to achieve satisfactory performance without using this technique.
- Controllers using wind scheduled set points (and possibly wind scheduled gains) necessitate of reliable measures of the wind blowing on the rotor. Mean wind estimates can be obtained by filtering anemometric measures; a possibly better approach is to use wind observers which obtain estimates of the wind from the response of the machine. The latter approach was used in the current study, obtaining consistently reliable mean wind estimates.

Acknowledgements

This work is supported in part from the Korea Institute of Energy and Resource Technology Evaluation and Planning (2008-N_BL-HM-E-08-0000).

References

- [1] Anonymous. Wind Turbines — Part 1: Design Requirements. Ed. 3.0, International Standard IEC 61400-1, 2005.
- [2] Anonymous. Wind Turbines — Part 2: Design Requirements for Small Wind Turbines. Ed. 2.0, International Standard IEC 61400-2, 2006.
- [3] Anonymous. Wind Turbine Generator System — Part 11: Acoustic noise measurement techniques. Ed. 2.1, International Standard IEC 61400-11, 2006.
- [4] Bauchau OA, Bottasso CL, Nikishkov YG. Modeling rotorcraft dynamics with finite element multibody procedures. *Mathematics and Computer Modeling* 2001; 33:1113-1137.

- [5] Bauchau OA, Bottasso CL, Trainelli L. Robust integration schemes for flexible multibody systems. *Computer Methods in Applied Mechanics and Engineering* 2003; 192:395–420.
- [6] Bossanyi EA. The design of closed loop controllers for wind turbines. *Wind Energy* 2000; 3(3):149–163.
- [7] Bottasso CL, Bauchau OA. On the design of energy preserving and decaying schemes for flexible, nonlinear multibody systems. *Computer Methods in Applied Mechanics and Engineering* 1999; 169:61–79.
- [8] Bottasso CL, Bauchau OA, Cardona A. Time-step-size-independent conditioning and sensitivity to perturbations in the numerical solution of index three differential algebraic equations. *SIAM Journal on Scientific Computing* 2007; 29:397–414.
- [9] Bottasso CL, Croce A. Advanced control laws for variable-speed wind turbines and supporting enabling technologies. Scientific Report DIA-SR 09-01, Dipartimento di Ingegneria Aerospaziale, Politecnico di Milano, Milano, Italy, January 2009.
- [10] Bottasso CL, Croce A. Cascading Kalman observers of structural flexible and wind states for wind turbine control. Scientific Report DIA-SR 09-02, Dipartimento di Ingegneria Aerospaziale, Politecnico di Milano, Milano, Italy, January 2009.
- [11] Garcia-Sanz M. Wind turbines: New challenges and advanced control solutions. *International Journal of Robust and Nonlinear Control* 2009; 19:1–3.
- [12] Jonkman JM, Buhl ML Jr. FAST User’s Guide. NREL/EL-500-29798, National Renewable Energy Laboratory, Golden, CO, USA, 2005.
- [13] Klug H. Noise from wind turbines — Standards and noise reduction procedures. *Forum Acusticum* 2002, Sevilla, Spain, 16–20 September 2002.
- [14] Leith DJ, Leithead WE. Appropriate realization of gain-scheduled controller with application to wind turbine regulation. *International Journal of Control* 1996; 65(2):223–248.
- [15] Leith DJ, Leithead WE, Survey of gain-scheduling analysis and design. *International Journal of Control* 2000; 73(11):1001–1025.

- [16] Leloudas G, JZhu, Sørensen JN, Shen WZ, Hjort S. Prediction and reduction of noise for a 2.3 MW wind turbine. *The Science of Making Torque from Wind*, Journal of Physics: Conference Series 2007; 75:1–9.
- [17] Ma X. Adaptive extremum control and wind turbine control. Ph.D. Thesis, Technical University of Denmark, 1997.
- [18] Ma X, Poulsen NK, Bindner H. Estimation of wind speed in connection to a wind turbine. Technical report, Technical University of Denmark, 1995.
- [19] Moerder D, Calise A. Convergence of a numerical algorithm for calculating optimal output feedback gains. *IEEE Transactions on Automatic Control* 1985; 30:900–903.
- [20] Mosca E. *Optimal, Predictive and Adaptive Control*. Prentice Hall, Englewood Cliffs, NJ, USA, 1995.
- [21] Østergaard KZ, Brath P, Stoustrup J. Estimation of effective wind speed. *Journal of Physics 2007: Conference series: The Science of Making Torque from Wind*; 75(012082).
- [22] Østergaard KZ, Stoustrup J, Brath P. Linear parameter varying control of wind turbines covering both partial load and full load conditions. *International Journal of Robust and Nonlinear Control* 2009; 19:92–116.
- [23] Peters DA, He CJ. Finite state induced flow models – Part II: three-dimensional rotor disk. *Journal of Aircraft* 1995; 32:323–33.
- [24] Powles SRJ. The effects of tower shadow on the dynamics of a horizontal-axis wind turbine. *Wind Engineering* 1983; 7:26–42.
- [25] Stol KA, Bir G. NWTC Design Codes, <http://wind.nrel.gov/designcodes/simulators/symdyn/>, last modified May 26, 2005; accessed August 18, 2008.
- [26] van der Hoof EL, Schaak P, van Engelen TG. Wind turbine control algorithms. Technical Report ECN-C-03-111, ECN Petten, December 2003.
- [27] van der Hooft EL, van Engelen TG. Estimated wind speed feed forward control for wind turbine operation optimisation. In *Proceedings of the European Wind Energy Conference*, London, U.K., 2004.